Available online at www.sciencedirect.com
SCIENCE DIRECT®
Remote Sensing of Environment 85 (2003) 410–423
Remote Sensing of Environment
www.elsevier.com/locate/rse

Effect of foliage spatial heterogeneity in the MODIS LAI and FPAR algorithm over broadleaf forests

N.V. Shabanov*, Y. Wang, W. Buermann, J. Dong, S. Hoffman, G.R. Smith, Y. Tian, Y. Knyazikhin, R.B. Myneni

Department of Geography, Boston University, 675 Commonwealth Avenue, Boston, MA 02215, USA

Received 9 January 2002; received in revised form 23 December 2002; accepted 31 December 2002

Abstract

This paper presents the analysis of radiative transfer assumptions underlying moderate resolution imaging spectroradiometer (MODIS) leaf area index (LAI) and fraction of photosynthetically active radiation (FPAR) algorithm for the case of spatially heterogeneous broadleaf forests. Data collected by a Boston University research group during the July 2000 field campaign at the Earth Observing System (EOS) core validation site, Harvard Forest, MA, were used for this purpose. The analysis covers three themes. First, the assumption of wavelength independence of spectral invariants of transport equation, central to the parameterization of the MODIS LAI and FPAR algorithm, is evaluated. The physical interpretation of those parameters is given and an approach to minimize the uncertainties in its retrievals is proposed. Second, the theoretical basis of the algorithm was refined by introducing stochastic concepts which account for the effect of foliage clumping and discontinuities on LAI retrievals. Third, the effect of spatial heterogeneity in FPAR was analyzed and compared to FPAR variation due to diurnal changes in solar zenith angle (SZA) to asses the validity of its static approximation.

Keywords: MODIS; LAI; FPAR; Stochastic radiative transfer; Vegetation remote sensing

1. Introduction

Leaf area index (LAI) and fraction of photosynthetically active radiation (0.4–0.7 μm) absorbed by vegetation (FPAR) are two key structural variables required in primary production models and global models of climate, hydrology, biogeochemistry, and ecology (Bonan, 1998; Dickinson, Henderson-Sellers, Kennedy, & Wilson, 1986; Running & Coughlan, 1988; Sellers et al., 1996). LAI and FPAR estimates are utilized by the Earth Observing System (EOS) Interdisciplinary Projects and other studies, typically in two ways (WWW 1): (1) as an eco-physiological measure of photosynthetic and transpirational surface within a vegetation canopy, and (2) as a remote sensing measure of the vegetation reflective surface within a canopy. While extensive measurements and studies of LAI and FPAR were made for small-stature vegetation such as agricultural crops and plantations, measurements and studies for natural ecosystems on global scale (such as forests and savannas) remain an open issue.

Remote sensing is a unique method for repetitive and relatively low-cost global monitoring of vegetation. Recently launched instruments such as the moderate resolution imaging spectroradiometer (MODIS) deliver a set of measurements for reliable estimates of vegetation canopy parameters including LAI and FPAR for use in model studies. An algorithm for the retrieval of LAI and FPAR from MODIS surface reflectrances was developed (Knyazikhin, Martonchik, Diner, et al., 1998; Knyazikhin, Martonchik, Myneni, Diner, & Running, 1998), prototyped prior to the launch of MODIS with AVHRR, Landsat TM, POLDER and SeaWiFS data (Tian et al., 2000; Wang et al., 2001; Zhang et al., 2000), and is in operational production since June 2000 (Myneni et al.,2002). Currently, an important activity is validation of this algorithm with field data. Validation, in general, refers to assessment of the uncertainty of higher-level satellite-sensor-derived products by comparison to reference data, which is presumed to represent the target value (Thomlinson, Bolstad, & Cohen, 1999). A key problem encountered in validation studies is the

* Corresponding author. Fax: +1-617-353-8399.
E-mail address: shabanov@bu.edu (N.V. Shabanov).

0034-4257/03/$ - see front matter © 2003 Elsevier Science Inc. All rights reserved.
doi:10.1016/S0034-4257(03)00017-8

highly discretized nature of land systems, which makes in situ measurement of coarse and moderate resolution parameters difficult. Consequently, evaluation of theoretical assumptions and parameterization of the algorithm can provide an initial indication of gross differences and possibly insights in to the reasons for the differences, however is not a substitute for validation of the product (Justice et al., 2000).

This paper describes the analysis of radiative transfer assumptions underlying MODIS LAI and FPAR algorithm for the case of broadleaf forests. Data collected by Boston University research group during July 2000 field campaign at the EOS core validation site, Harvard Forest, MA (WWW 2) were used for this purpose. The data set includes a detailed sampling of LAI, PAR, canopy spectral transmittances and reflectances, soil and understory spectral reflectances, and leaf optical properties of key species. The additional information about validation of LAI and FPAR algorithm over several types of vegetation is provided at separate publications (Privette et al., 2002; Tian et al., 2002 (a,b); Wang et al., in preparation).

The paper is organized as follows. In the first section, the Harvard Forest site and the measurements are described. The next section introduces spectral invariants, central theoretical assumption of the LAI and FPAR algorithm. The physical interpretation of those parameters is given and an approach to minimize the uncertainties in its retrievals is proposed. The following section introduces representation of these invariants according to stochastic radiative transfer theory to account for the effect of foliage clumping and discontinuities on LAI retrievals. In the last section the effect of spatial heterogeneity in FPAR was analyzed and compared to FPAR variation due to diurnal changes in solar zenith angle to assess the validity of static representations of FPAR. The conclusions are summarized at the end.

2. The experimental site, instrumentation and measurements

2.1. Site description

The Harvard Forest is a 3000-acre site, located 42.5382° North and 72.1714° West, in Petersham, MA, USA. The site has a transition land cover dominated by mixed hardwood and conifer forests, ponds, extensive spruce and maple swamps. Harvard Forest is well known for its long history of scientific research of monitoring natural disturbances, environmental change and human impacts (WWW 3). This site was selected for several recent major field campaigns within following projects: BigFoot, Flux Network (FLUXNET), Global Landcover Test Site Initiative (GLCTS), Long-Term Ecological Research (LTER). It is also an EOS core validation site, selected to provide a focus for satellite, aircraft, and ground data collection of land product validation (WWW 1).

2.2. Data sampling

The Climate and Vegetation Research Group of Boston University performed a field campaign at the Harvard Forest, July 21–25, 2000. The emphasis was on collection of LAI, PAR, spectral transmittance and reflectance as well as leaf optical properties of key species for validation of the theoretical basis of the MODIS LAI and FPAR algorithm (Knyazikhin, Martonchik, Myneni, et al., 1998). Data were collected primarily on a 225 × 225-m grid over a relatively flat terrain just outside the southeast boundary of the Harvard Forest. This grid was delimited by a matrix of nine rows labeled "1–9" and nine columns, labeled "A–I", for a total of 81 points. Thus, each grid-centered point was located 25 m from its neighbors. The columns were oriented magnetic north to south, with rows running perpendicularly (cf. Fig. 1). The grid center is located at UTM coordinates of zone 18, 732,097 m E, 4,712,915 m N. Additionally several measurements were performed along transects of about 100 m. Data were acquired with ASD, LAI-2000, LI-1800 and AccuPAR ceptometers at each grid cell (no endorsement of commercial products intended here or elsewhere).

The *LI-1800 Spectroradiometer* with a standard cosine receptor and fitted with a LI-1800-12 External Integrating Sphere was used to measure leaf spectral hemispherical transmittances and reflectances. The spectra were measured in the 400–1100-nm range at 1-nm resolution on leaf

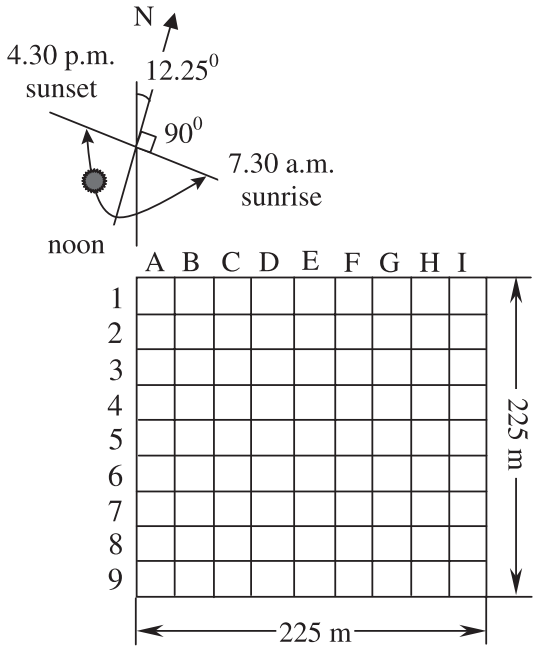

Fig. 1. Schematic plot of the grid site at the Harvard Forest. The site is delimited by a matrix of nine rows labeled "1–9" and nine columns, labeled "A–I". Each cell is 25 × 25 m resulting in a 225 × 225-m grid. The columns are oriented magnetic north to south, with rows running perpendicularly. The movement of the sun through the day is indicated. The data were collected during July 21–25, 2000.

samples taken from six dominant broadleaf forest species (sugar maple, red oak, American beech, viburnum, American chestnut, birch).

The *ASD-spectroradiometer* was used to measure canopy hemispherical spectral transmittances and soil/undersory reflectances (each spectrum consisting of 512 measurements from 282.79 to 1085.72 nm). Measurements were made using hemispherical fore-optics. The sensor was held horizontal over the ground at a minimum height of 1 m (also above the local understory) and measurements of spectral upward and downward fluxes were taken at each grid cell and in the open area. Every spectrum represents an average of three separate measurements made in close proximity of the grid cell centers. The raw DNs were converted to radiances followed by translation to canopy transmittances or soil/understory reflectances.

The *LAI-2000 plant canopy analyzer* was used to measure the LAI and directional gap fraction. The sensor projects a nearly hemispheric image on to five detectors arranged in concentric rings (approximately 0–13°, 16–28°, 32–43°, 47–58° and 61–74°). Radiation above 490 nm is rejected from analysis. A one-fourth cover cap was placed over both sensors to prevent operator interference. LAI measurements were collected early morning and late afternoon under diffuse sky conditions. The sensor was held above the local understory at a minimum height of 1 m. Every data point represents an average of three separate measurements made in close proximity of the grid cell centers.

AccuPAR ceptometers were used to monitor incident PAR with observations recorded every 3 min.

Some sample leaf and canopy spectra are shown in Fig. 2. The canopy and soil spectra acquired at different values of LAI are shown because of high spatial variability of the measurements. The analysis was done by splitting the range of observed LAI [0–6.5] into 10 equally spaced bins of $\Delta LAI = 0.65$, $LAI \in \{2.9, 3.6, 4.2, 4.9, 5.5, 6.2\}$. For each LAI-bin, grid cell(s) with measured LAI values in the bin were identified, that is, $LAI \in [LAI^*, LAI^* + \Delta LAI]$. When each grid cell was associated with a particular bin, the corresponding bin quantities were then averaged. In this fashion, we establish typical or standard values for use in subsequent analysis.

3. Evaluation of spectral invariants and their uncertainties

The MOD15A2 product (LAI, FPAR, and associated Quality control) is produced by the MODIS LAI and FPAR algorithm (Knyazikhin, Martonchik, Myneni, et al., 1998). The algorithm accomplishes an inverse solution of the three-dimensional radiative transfer equation using Look-Up-Tables (Knyazikhin, Martonchik, Diner, et al., 1998; Knyazikhin, Martonchik, Myneni, et al., 1998). A key idea to optimize Look-Up-Tables is the use of eigenvalues derived in the transport theory to relate optical properties of indi-

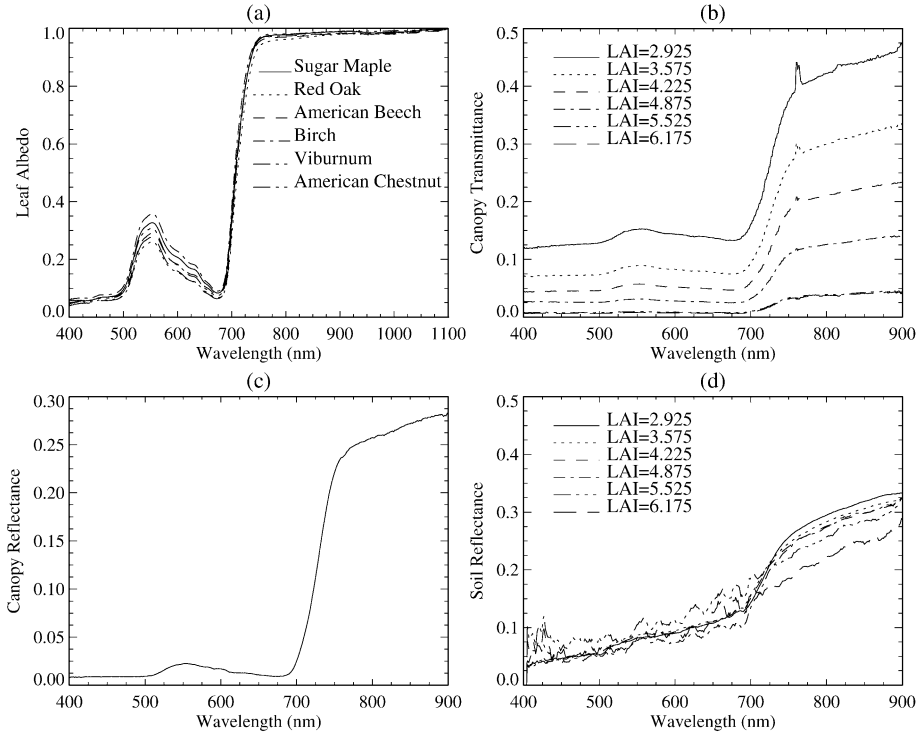

Fig. 2. Spectral data collected at the grid site. Panel (a) shows the spectral leaf albedo of six predominant species. Panel (b) shows spectral canopy transmittance averaged over grid cells of six LAI classes. Panel (c) shows spectral canopy reflectance measured from a fire tower. Panel (d) shows spectral soil and understory reflectance averaged over six LAI classes.

vidual leaves to vegetation canopy transmittance and absorptance. For a vegetation canopy bounded at its bottom by a black surface, the dependence of canopy transmittance, $t(\lambda)$, on wavelength, λ, is described by (Knyazikhin, Martonchik, Diner, et al., 1998; Panferov et al., 2001)

$$t(\lambda) = t(\lambda_{\text{ref}}) \cdot \frac{1 - p_t \cdot \omega(\lambda_{\text{ref}})}{1 - p_t \cdot \omega(\lambda)}. \quad (1)$$

Here $t(\lambda_{\text{ref}})$ and $\omega(\lambda_{\text{ref}})$ are the canopy transmittance and leaf albedo at an arbitrary chosen reference wavelength, λ_{ref}. The parameter p_t is the eigenvalue (normalized by leaf albedo) of the linear operator that assigns downward radiances at the canopy bottom to incoming radiation, representing the transmittance process (Panferov et al., 2001). This parameter depends on solar zenith angle, leaf area index, L, canopy structure, and the ratio of leaf transmittance, $t_{\text{leaf}}(\lambda_{\text{ref}})$, to leaf albedo, $\omega(\lambda_{\text{ref}})$ at λ_{ref}. Solving Eq. (1) for p_t yields

$$p_t = \frac{t(\lambda_1) - t(\lambda_2)}{\omega(\lambda_1) \cdot t(\lambda_1) - \omega(\lambda_2) \cdot t(\lambda_2)} = \text{const}, \forall \lambda_1, \lambda_2. \quad (2)$$

This equation can be used to estimate p_t from field measurements of canopy transmittance and leaf albedo. Also, taking $\omega(\lambda_{\text{ref}}) = 0$ in Eq. (1), one obtains the following relationship between uncollided radiation arriving at the canopy bottom, $q_t \equiv t(\omega(\lambda_{\text{ref}}) = 0)$, and the total transmitted radiation $t(\lambda)$,

$$q_t = t(\lambda) \cdot [1 - \omega(\lambda) \cdot p_t], \forall \lambda. \quad (3)$$

The product $\omega(\lambda) \cdot p_t$ has fundamental physical meaning: it defines the portion of collided radiation, $t(\lambda) - q_t$, in total transmitted radiation, $t(\lambda)$,

$$\frac{t(\lambda) - q_t}{t(\lambda)} = \omega(\lambda) \cdot p_t, \forall \lambda.$$

The derivation of Eq. (3) from the radiative transfer equation is given in Appendix B. In classical radiative transfer theory, uncollided radiation in a given direction, Q, is described by the Beer's law (Ross, 1981). For a horizontally homogeneous canopy with black (completely absorbing) leaves above a black soil, uncollided radiation in a given direction normalized by the incident flux density, under diffuse illumination conditions is given by,

$$Q(L, \theta) = \frac{1}{\pi} \cdot \exp\left[-\frac{G(\theta) \cdot L}{\mu(\theta)}\right], \qquad \theta \in \left[\frac{\pi}{2}; \pi\right]. \quad (4)$$

Here $\mu(\theta)$ is the absolute value of the cosine of solar zenith angle, $G(\theta)$ is the mean projection of leaf normals to the

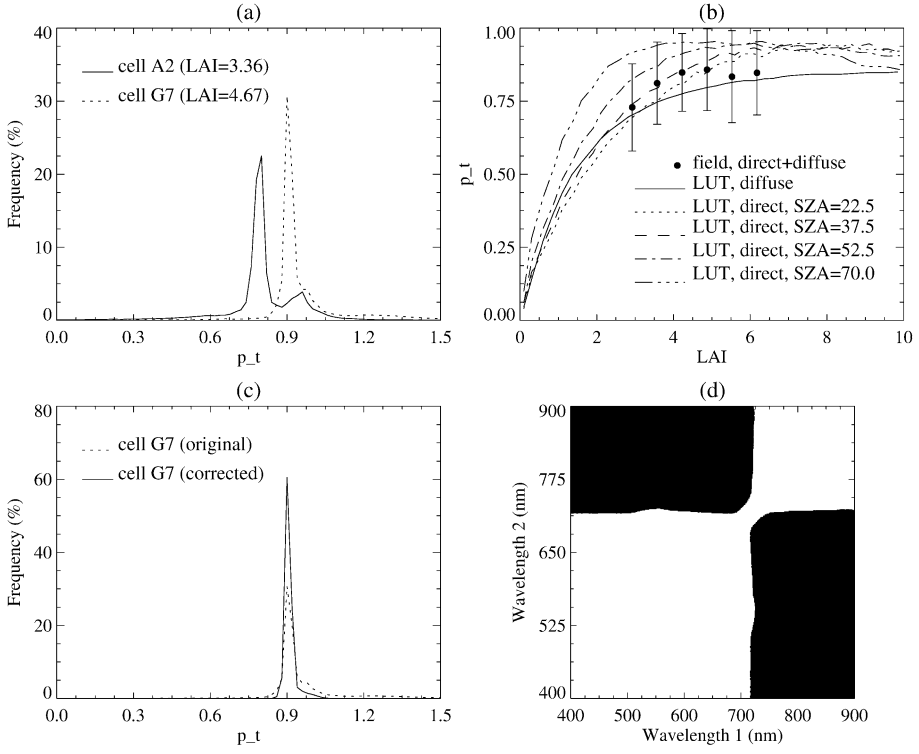

Fig. 3. Retrievals of the parameter p_t. Panel (a) shows example retrieval p_t for two grid cells (A2 and G7). Panel (b) shows LAI dependence of p_t for six LAI classes (dots with error bars). Also shown is the dependence of p_t on LAI values stored in the MODIS LAI and FPAR algorithm's Look-Up-Tables. The LUTs include several p_t curves for vegetation illuminated by direct sunlight from different angles (four curves) and an additional curve for diffuse radiation. Panel (c) shows increase in the accuracy of p_t retrieval when spectral screening is applied. Panel (d) shows the space of all possible wavelength locations where p_t is localized accurately (denoted in black).

direction θ and L is the leaf area index. The q_t parameter is hemispherically integrated Q,

$$q_t = 2\pi \cdot \int_0^1 Q(L,\theta) \cdot \mu(\theta) \mathrm{d}\mu. \quad (5)$$

We utilize the data collected by the Boston University research group (leaf albedo from LI-1800, transmitted radiation from ASD and LAI from LAI-2000) at the grid site (Fig. 1) to evaluate q_t and p_t parameters. Given the spectra of canopy transmittance and leaf albedo (Fig. 2a), histograms of p_t for each grid cell are first evaluated. Two example histograms are shown in Fig. 3a, for grid cell A-2 (LAI = 3.36, $\bar{p}_t = 0.80$) and G-7 (LAI = 4.67, $\bar{p}_t = 0.90$). The p_t value corresponding to the mean of the distribution for each grid cell is used to calculate the corresponding q_t histogram and mean value (Fig. 5b). For grid cell A-2, $\bar{q}_t = 0.080$ and for G-7, $\bar{q}_t = 0.012$. In the ideal case of null uncertainties, the histograms resemble delta functions in view of wavelength independence of these parameters. Comparing histograms of p_t and q_t parameters, one should note that p_t is better localized and q_t is more sensitive to LAI for the broadleaf forest at Harvard forest.

Eq. (1) states that canopy transmittance at any wavelength can be evaluated from estimates of canopy transmittance, leaf transmittance and leaf albedo at arbitrary chosen reference wavelength λ_{ref}. Fig. 4a shows validation of this formula for grid cell G-7, for reference wavelength $\lambda_{ref} = 714$ nm, $\omega(\lambda_{ref}) = 0.63$ and $t(\lambda_{ref}) = 0.032$ and $p_t = 0.90$. The fit is uniformly good in the wavelength range 400–800 nm. At 800 nm, the leaf albedo reaches a high value of 0.978 (Fig. 2a), and the relationship between canopy transmittance and leaf albedo becomes undefined (cf. Fig. 4b). In order to accurately localize a value of p_t, the ratio t_{leaf}/ω should be a single-value function with respect to ω (Panferov et al., 2001). This condition is not well obeyed in the interval $0.1 < \omega < 0.25$ where t_{leaf}/ω takes on multiple values (Fig. 4b).

As mentioned before, the parameters q_t and p_t depend on LAI and this can be assessed with the available field data in the LAI range 3–6. The average spectra of canopy transmittance and leaf albedo (Fig. 2) are used to establish the relationship $t = f(\omega)$ between canopy transmittance t and leaf albedo ω. Probable values of q_t and p_t are then estimated from the resulting histograms, as described before.

The dependence of p_t on LAI is shown in Fig. 3b. The parameter p_t increases with LAI. This parameter is stored in the MODIS LAI and FPAR algorithm Look-Up-Tables, separately for diffuse incident radiation and for direct radiation at different solar zenith angles {22.5°, 37.5°, 52.5°, 70.0°}, which is also shown in Fig. 3b. The parameter values evaluated from field measurements are within the range of values used in the MODIS algorithm. The field-based p_t values are close to theoretical values for diffuse radiation, which is reasonable, as the transmittance measurements were made under mostly cloudy skies (Fig. 5a).

The dependence of q_t on LAI evaluated with canopy transmittance data, leaf albedo and measured LAI according to Eq. (3) is shown in Fig. 5c (marked 'ASD data'). This parameter can also be evaluated from uncollided radiation [cf. Eq. (5)] estimated from gap fraction measurements of LAI-2000. The gap fraction $P(\theta)$ observed along θ is the ratio of uncollided radiation $Q(\theta)$ to the incident flux density,

$$P(\theta) = \frac{Q(L,\theta)}{1/\pi}. \quad (6)$$

Thus, according to Eq. (5),

$$q_t = 2 \cdot \int_0^1 P(\theta) \cdot \mu(\theta) \mathrm{d}\mu.$$

The resulting estimation of q_t is also shown in Fig. 5c (marked 'LAI-200 data'). This curve must be considered as more reliable because all data were obtained from a single instrument under identical atmospheric conditions and the effect of spatial heterogeneity is also minimized.

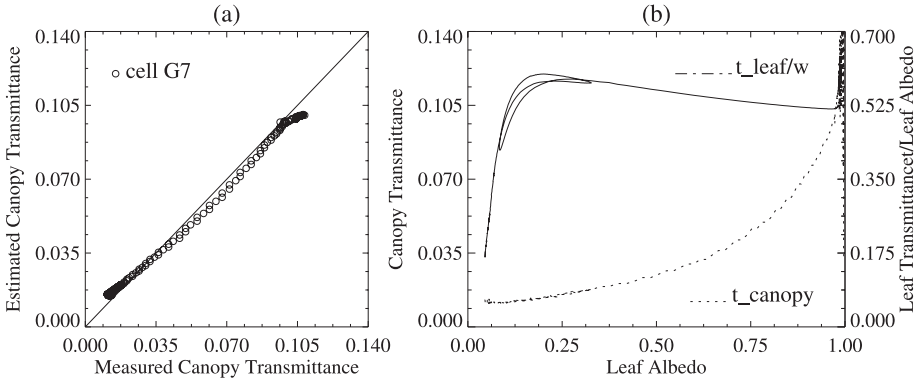

Fig. 4. Panel (a) shows comparison of spectral canopy transmittance retrievals with measured values for grid cell G7. Panel (b) shows the dependence of spectral canopy transmittance on spectral leaf albedo for grid cell G7 (t_{canopy}, dotted line). Also shown is the ratio of leaf spectral transmittance to leaf spectral albedo as a function of leaf spectral albedo (t_{leaf}/ω, solid line) for grid cell G7.

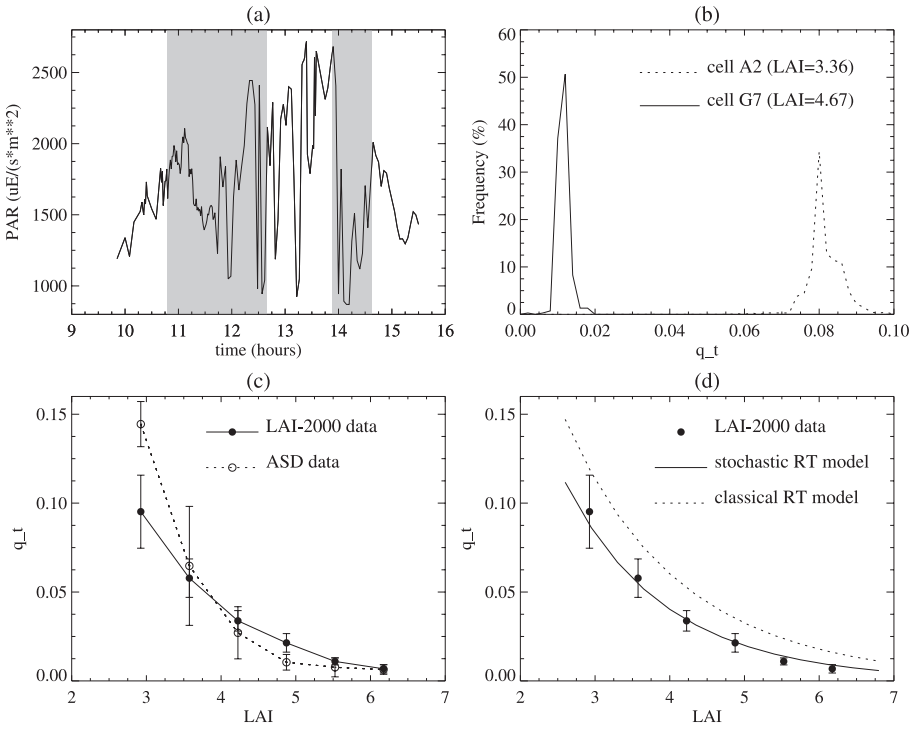

Fig. 5. Retrievals of the parameter q_t. Panel (a) shows atmospheric conditions during the day. Panel (b) shows example retrieval of q_t parameter for two grid cells (A2 and G7). Panel (c) shows the dependence of q_t on LAI estimated by two methods from field data: (1) the solid line shows estimation based on LAI-2000 data, (2) the dashed line shows estimation based on ASD data. Panel (d) shows modeling of the q_t parameter with classical RT model (dotted line), stochastic RT (solid line) and q_t from LAI-2000 data (dots with error bars).

The theoretical relationship between q_t and LAI based on Eqs. (4) and (5), shown in Fig. 5d, is an overestimation. The empirical relations are steeper, possibly due to clumping, which is not captured in a homogeneous representation of the vegetation canopy (cf. next section).

We now address the issue of uncertainties in empirical estimates of these spectral invariants. There are several reasons for these uncertainties. One main reason is spatial heterogeneity, that is, vegetation structural properties vary significantly even at scales smaller than 1 m in the stand. Ideally, all measurements required for the estimation of p_t and q_t should be measured simultaneously at the same spatial location. Another reason is undersampling—this is especially true for leaf optical properties. Several species are generally present, even at any "one" location, and the ratio of species is difficult to determine. One generally uses the properties of the predominant species. Also, Eq. (2) was derived under the assumption of totally absorbing background, which is violated at the grid site (cf. Fig. 2d). Further, instrument errors and numerical approximations introduce additional uncertainties. Finally, uncertainties in estimates of q_t are significantly higher than for p_t, because the statistics for the histogram of q_t contain significantly fewer points than for p_t [N versus $N\cdot(N-1)/2$, where N is the number of spectral measurements, 687].

How to minimize these uncertainties? We discuss this in the context of estimation of p_t [cf. Eq. (2)]. Clearly, uncertainties arise because the functional relationship $t=f(\omega)$ is established in practice always with some level of noise. Therefore, p_t will not be exactly localized from measurements of all possible wavelength couples, $\{\lambda_1, \lambda_2\}$. However, a subset of these wavelength pairs $\{\lambda_1, \lambda_2\}$ can be chosen such that the error in the estimation of p_t can be minimized. Consider two estimations of p_t, where leaf albedo is defined with uncertainties $\Delta\omega$ [that is uncertainties in the relation $t=f(\omega)$]:

$$p_t = \frac{t_1 - t_2}{\omega_1 \cdot t_1 - \omega_2 \cdot t_2},$$

and

$$p_t^* = \frac{t_1 - t_2}{(\omega_1 + \Delta\omega) \cdot t_1 - (\omega_2 + \Delta\omega) \cdot t_2}.$$

The relative error in the estimation of p_t will be

$$\varepsilon \equiv \mathrm{Max}\left\{\frac{p_t - p_t^*}{p_t^*}\right\} = \frac{\Delta\omega \cdot (t_1 + t_2)}{\omega_1 \cdot t_1 - \omega_2 \cdot t_2}. \quad (7)$$

Now, note that $t=f(\omega)$ is monotonical, as ω increases, t increases as well (cf. Fig. 4b). Therefore, to minimize uncertainties in p_t, one must consider only those wavelength pairs for which the leaf albedo, and therefore canopy transmittance, change significantly (larger then variations in soil reflectance), but the sum of transmittances must be minimal. One choice would be to select wavelength pairs separated widely, for instance, one in the visible portion of the

spectrum and the other in the near-infrared. Another choice is to select very nearly spaced wavelength pairs between 700 and 750 nm where spectral properties change significantly. This is illustrated in Fig. 3d, where the masked regions correspond to 'good' combinations of wavelengths. In this region, the relative error $\varepsilon/\Delta\omega$ is 1.45.

4. Improved theoretical representation of spectral invariants

4.1. Stochastic equations for uncollided radiation

The spectral invariant q_t is hemispherically integrated uncollided radiation, which in classical radiative transfer theory is described by the Beer's law. The standard parameterization is inadequate for dealing with foliage distribution discontinuities and clumping of vegetation elements (Shabanov, Knyazikhin, Baret, & Myneni, 2000). An accurate description of uncollided radiation requires stochastic description. Based on our previous research (Shabanov et al., 2000), an equation for Q in the case of discontinuous media can be formulated as,

$$Q^{\mathrm{U}}(L,\theta)+\frac{G(\theta)}{\mu(\theta)}\cdot\int_0^L\frac{K(L,\xi,\theta)}{p(\xi)}\cdot Q^{\mathrm{U}}(\xi,\theta)\mathrm{d}\xi=\frac{1}{\pi},\quad \theta\in\left[\frac{\pi}{2};\pi\right], \tag{8}$$

where $Q^{\mathrm{U}}(L,\theta)$ is uncollided radiation averaged over that portion of a horizontal plane occupied by vegetation at depth L [equivalent to $Q(\mathrm{L},\theta)$ in classical theory], $p(\xi)$ is the probability of finding foliage elements on the horizontal plane ξ, and the kernel $K(L,\xi,\theta)$ is the correlation between foliage elements located at L and ξ along the direction θ. Reliable estimates of $G(\theta)$ can be derived from field data, for example, from LAI-2000 angular measurements. The next section describes one such method, from which it will be established that $G(\theta)=0.5$ for all angles θ.

We adopt a model proposed by Vainikko (1973) for the kernel, where the medium is assumed to be vertically homogeneous [$p(\xi)\equiv p$]. The following model of the kernel describes horizontal heterogeneity,

$$K(L,\xi,\theta)=\exp\left[-\frac{a\cdot|L-\xi|}{\mu(\theta)}\right]\cdot(1-p)+p, \tag{9}$$

where $1/a$ is the mean radius of correlation between elements in the medium. For this analytic kernel, the explicit solution is (Vainikko, 1973)

$$Q^{\mathrm{U}}(L,\theta)=\frac{1}{\pi\cdot(\lambda_2-\lambda_1)}\cdot\left\{(G(\theta)/p-\lambda_1)\cdot\exp\left[-\frac{\lambda_2\cdot L}{\mu(\theta)}\right]+(\lambda_2-G(\theta)/p)\cdot\exp\left[-\frac{\lambda_1\cdot L}{\mu(\theta)}\right]\right\}, \tag{10}$$

where

$$\lambda_{1,2}=\frac{G(\theta)/p+a}{2}\pm\frac{\sqrt{(G(\theta)/p+a)^2-4\cdot a\cdot G(\theta)}}{2}. \tag{11}$$

Let $a=0$, which corresponds to the case of uniform correlation with distance, that is, points located near each other are correlated as strongly as with remote points. This could be the case in heterogeneous media, where it is just as easy to find clumps of vegetation near a location, or farther away. In this case, the kernel simplifies, $K(L,\xi,\theta)\equiv 1$, and we have the following expression for uncollided radiation,

$$Q^{\mathrm{U}}(L,\theta)=\frac{1}{\pi}\cdot\exp\left[-\frac{G(\theta)\cdot L}{p\cdot\mu(\theta)}\right], \tag{12}$$

which is similar to Eq. (4) derived in standard theory, with the exception of the probability of finding foliage elements, p, in the exponent. The classical expression, Eq. (4), was modified in several works (e.g., Chen, 1996; Chen, Rich, Gower, Norman, & Plummer, 1997; Nilson, 1971), by introducing a so-called clumping coefficient on an ad hoc basis. The coefficient $1/p$ corresponds to a clumping coefficient. An important question is, what does the LAI-2000 measure? Do the reported LAI values correspond to L or L/p? The instrument assumes classical representation, that is Eq. (4), so it reports effective classical LAI, that is $L^{\mathrm{classical}}=L/p$. To obtain the leaf area index, the effective value should be multiplied by p, $p\cdot L^{\mathrm{classical}}$.

The concept of gaps or discontinuities is a key element of stochastic RT theory in contrast to classical RT theory. In stochastic theory, LAI is defined as (Shabanov et al., 2000),

$$L=d_{\mathrm{L}}\cdot\int_0^H p(z)\mathrm{d}z,$$

where H is the height of canopy, d_{L} is leaf area density, one-sided leaf area per unit volume (in $\mathrm{m}^2/\mathrm{m}^3$). Assuming that the probability of finding foliage elements does not depend on height, $p(z)=p$,

$$L=d_{\mathrm{L}}\cdot\int_0^H p(z)\mathrm{d}z=p\cdot d_{\mathrm{L}}\cdot H\equiv p\cdot L^{\mathrm{classical}}.$$

Consider Fig. 5d, which shows field estimates of q_t from LAI-2000 data, together with those predicted by classical and stochastic transport theories [cf. Eqs. (5) and (12)]. The value of p used in these calculations was 0.86, obtained from best fit to the field data. Thus, the whole procedure of retrieving LAI is restricted to LAI-2000 data only. Note also that LAI-2000 data were used as they result in more reliable estimates of q_t compared to ASD data, because the atmospheric conditions were not stable. The dependence of q_t on LAI is modeled better with stochastic theory because horizontal discontinuities, gaps and clumping are explicitly included.

4.2. Retrieval of leaf normal orientation

In the previous section, we have seen that stochastic equations provide the proper parameterization required for the description of foliage clumping and its effect on uncollided radiation. Eq. (12) depends on two parameters: (1) p, the fraction of foliage elements, and (2) the G-function. We estimated the first parameter from model fits to field data, assuming that $G=0.5$ for all zenith angles at the Harvard Forest grid site. In this section, this assumption is tested. Specifically, we formulate a method, consistent with stochastic theory, for estimates of leaf normal orientation distribution and G-function from measurements of gap fraction under the canopy.

This approach is based on the method of point quadrats introduced by Wilson (1960) and further developed by Miller (1964, 1967). Consider the gap fraction $P(\theta)$ as seen from below the canopy. It follows from Eqs. (6) and (12) that

$$P(\theta)=\exp\left[-\frac{G(\theta)\cdot L}{p\cdot\mu(\theta)}\right]. \tag{13}$$

The mean projection of leaf normals to the direction θ, the function $G(\theta)$, on the assumption of azimuthally independent orientation of leaf normals, is given by (Ross, 1981)

$$G(\theta)=\frac{1}{2\pi}\cdot\int_{2\pi^+} g_{\mathrm{L}}(\theta_{\mathrm{L}})\cdot\left|\vec{\Omega}\cdot\vec{\Omega}_{\mathrm{L}}\right|\mathrm{d}\vec{\Omega}_{\mathrm{L}}, \tag{14}$$

where $g_{\mathrm{L}}(\theta_{\mathrm{L}})$ is the probability density of leaf normal orientations over the upper hemisphere, and

$$\frac{1}{2\pi}\cdot\int_{2\pi^+} g_{\mathrm{L}}(\theta_{\mathrm{L}})\mathrm{d}\vec{\Omega}_{\mathrm{L}}=1. \tag{15}$$

The function $G(\theta)$, importantly, satisfies the constraint

$$\int_0^{\pi/2}\sin(\theta)\cdot G(\theta)\mathrm{d}\theta=\frac{1}{2}. \tag{16}$$

In the case of azimuthally symmetric g_{L},

$$\begin{aligned}&\frac{1}{2\pi}\cdot\int_{2\pi^+} g_{\mathrm{L}}(\theta_{\mathrm{L}})\cdot\left|\vec{\Omega}\cdot\vec{\Omega}_{\mathrm{L}}\right|\mathrm{d}\vec{\Omega}_{\mathrm{L}}\\&=\int_0^{\pi/2}\mathrm{d}\theta_{\mathrm{L}}\sin(\theta_{\mathrm{L}})\cdot g_{\mathrm{L}}(\theta_{\mathrm{L}})\frac{1}{2\pi}\int_0^{2\pi}\mathrm{d}\varphi_{\mathrm{L}}\left|\vec{\Omega}\cdot\vec{\Omega}_{\mathrm{L}}\right|\\&=\int_0^{\pi/2}\mathrm{d}\theta_{\mathrm{L}}\sin(\theta_{\mathrm{L}})\cdot g_{\mathrm{L}}(\theta_{\mathrm{L}})\psi(\theta,\theta_{\mathrm{L}}),\end{aligned} \tag{17}$$

where (Knyazikhin & Marshak, 1991)

$$\psi(\theta,\theta_{\mathrm{L}})=\begin{cases}\left|\cos(\theta)\cdot\cos(\theta_{\mathrm{L}})\right|, & \text{if } \left|\mathrm{ctg}(\theta)\cdot\mathrm{ctg}(\theta_{\mathrm{L}})\right|>1\\ \left|\frac{2}{\pi}\cdot\sin(\theta)\cdot\sin(\theta_{\mathrm{L}})\cdot\sin(\varphi^*)+\cos(\theta)\cdot\cos(\theta_{\mathrm{L}})\cdot\left(\frac{2\cdot\varphi^*}{\pi}-1\right)\right|, & \text{if } \left|\mathrm{ctg}(\theta)\cdot\mathrm{ctg}(\theta_{\mathrm{L}})\right|<1\end{cases} \tag{18}$$

and

$$\varphi^*=\arccos[-\mathrm{ctg}(\theta)\cdot\mathrm{ctg}(\theta_{\mathrm{L}})].$$

Substituting Eqs. (14) and (17) into Eq. (13) results in

$$P(\theta)=\exp\left[-\frac{L}{p\cdot\cos(\theta)}\cdot\int_0^{\pi/2}\sin(\theta_{\mathrm{L}})\cdot g_{\mathrm{L}}(\theta_{\mathrm{L}})\cdot\psi(\theta,\theta_{\mathrm{L}})\mathrm{d}\theta_{\mathrm{L}};\right], \tag{19}$$

or

$$\int_0^{\pi/2}\tilde{\psi}(\theta,\theta_{\mathrm{L}})\cdot\tilde{g}_{\mathrm{L}}(\theta_{\mathrm{L}})\mathrm{d}\theta_{\mathrm{L}}=\ln\left(\frac{1}{P(\theta)}\right), \tag{20}$$

where $\tilde{\psi}(\theta,\ \theta_{\mathrm{L}})=\psi(\theta,\ \theta_{\mathrm{L}})\cdot\sin(\theta_{\mathrm{L}})/\cos(\theta)$ and $\tilde{g}_{\mathrm{L}}(\theta_{\mathrm{L}})=(L/p)\cdot g_{\mathrm{L}}(\theta_{\mathrm{L}})$. Eq. (20) is a Fredholm integral equation of first kind with respect to the unknown function $\tilde{g}_{\mathrm{L}}(\theta_{\mathrm{L}})$ and the kernel $\tilde{\psi}(\theta,\ \theta_{\mathrm{L}})$. Solving this equation results in the leaf area index L and leaf normal distribution $g_{\mathrm{L}}(\theta_{\mathrm{L}})$, taking into account the normalization of $g_{\mathrm{L}}(\theta_{\mathrm{L}})$ (Eq. (15)), that is,

$$\frac{L}{p}=\int_0^{\pi/2}\sin(\theta_{\mathrm{L}})\cdot\tilde{g}_{\mathrm{L}}(\theta_{\mathrm{L}})\mathrm{d}\theta_{\mathrm{L}}, \tag{21}$$

$$g_{\mathrm{L}}(\theta_{\mathrm{L}})=\frac{\tilde{g}_{\mathrm{L}}(\theta_L)}{L/p}. \tag{22}$$

The critical step is to find an appropriate method to solve Eq. (21) numerically. A straightforward matrix approximation of Eq. (20) gives poor solutions, irrespective of the order of quadrature used to approximate the integral. The reasons are: (1) solution of the Fredholm integral equation of the first kind is an ill-posed problem; the corresponding linear operator has no bounded inverse; (2) errors in the estimation of the right-hand side of Eq. (20). Therefore, we adopt a regularization approach (Tikhonov & Arsenin, 1977) for solving Eq. (20). We rewrite Eq. (20) in operator form as

$$\hat{\mathbf{A}}\mathbf{f}=\mathbf{g},$$

where $(\hat{\mathbf{A}})_{ij}=\mathbf{w}_i\psi_{ij}$ $(i,j=0,..n)$ is the discrete form of the left-hand side of Eq. (20) and g_i is the discrete form of the

right-hand side. Because **g** is known in practice only with a certain level of uncertainty, we have in effect

$$\hat{\mathbf{A}}\mathbf{f} = \mathbf{g} + \varepsilon.$$

The problem is solved by introducing a regularization operator and searching for the smoothest solution, $\mathbf{f}_{\text{smooth}}$,

$$\mathbf{f}_{\text{smooth}} = (\hat{\mathbf{A}} + \gamma \cdot \hat{\mathbf{B}})^{-1}\mathbf{g},$$

where for $(i, j = 0, \ldots n)$, the matrix $(\hat{\mathbf{B}})_{ij}$ defined as follows (Phillips, 1962),

$$(\hat{\mathbf{B}})_{ij} \equiv (\hat{\mathbf{A}}^{-1})_{j-2,i} - 4 \cdot (\hat{\mathbf{A}}^{-1})_{j-1,i} + 6 \cdot (\hat{\mathbf{A}}^{-1})_{j,i} - 4 \cdot (\hat{\mathbf{A}}^{-1})_{j+1,i} + (\hat{\mathbf{A}}^{-1})_{j+2,i},$$

and

$$(\hat{\mathbf{A}}^{-1})_{-2,i} = -(\hat{\mathbf{A}}^{-1})_{0,i},$$

$$(\hat{\mathbf{A}}^{-1})_{-1,i} = 0,$$

$$(\hat{\mathbf{A}}^{-1})_{n+1,i} = 0,$$

$$(\hat{\mathbf{A}}^{-1})_{n+2,i} = -(\hat{\mathbf{A}}^{-1})_{n,i}.$$

Note, similar technique was implemented by Norman and Campbell (1989), but without considering clumping. The choice of the regularization parameter γ is somewhat arbitrary as the solution is not very sensitive to γ. Generally, γ is related to uncertainty ε in g. In our calculations, we choose $\gamma = 0.5$. In general, an important source of error associated with LAI and leaf normal distribution retrieval from numerical solution of the Fredholm equation is due to sparse angular sampling of $P(\theta)$ (polar angles 7, 23, 38, 53, 68, in degrees, in the case of LAI-2000).

We evaluate the proposed scheme by comparing the retrieved LAI with that obtained from the Miller's (1967) formula currently used by the LAI-2000. Miller's formula can be obtained by extracting $G(\theta)$ from Eq. (13) and substituting into Eq. (16),

$$\frac{L}{p} = 2 \cdot \int_0^1 \ln\left(\frac{1}{P(\theta)}\right) \cdot \mu(\theta) \mathrm{d}\mu. \tag{23}$$

Note that the Miller's formula combined with Eq. (16) does not provide a reliable estimate of $G(\theta)$ [substituting LAI from Eq. (23) into Eq. (13) and inversion for $G(\theta)$]. This is because the Fredholm equation-based method incorporates the entire set of angular information for retrieval of $G(\theta)$ and while the Miller's method does not.

We implemented a numerical scheme for the solution of the Fredholm equation, with gap fractions from the LAI-2000 measured at the grid experiment in the Harvard Forest. The retrievals obtained by the Fredholm and Miller's equations are shown in Fig. 6. The retrieved LAI values compare quite favorably (Fig. 6a) and so do the distributions

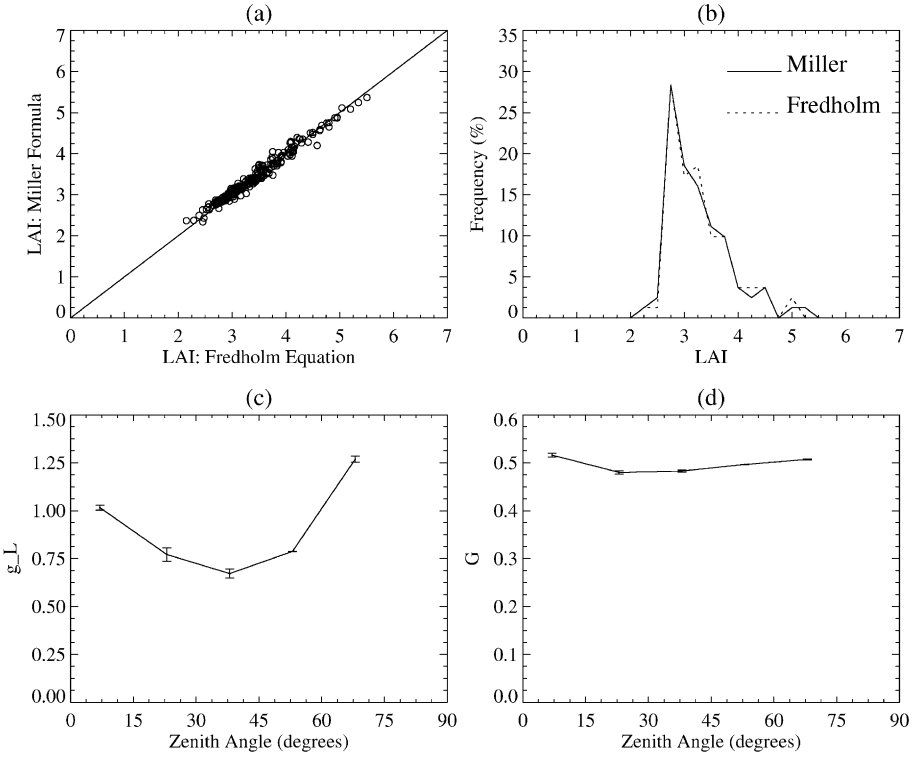

Fig. 6. The Fredholm integral equation method for LAI and leaf normal orientation retrieval. Panel (a) is one-to-one comparison of LAI retrieved by the Fredholm integral equation method and the standard method utilized by LAI-2000 (Miller's formula). Panel (b) shows the distribution of LAI values derived by two methods. Panel (c) shows estimation of leaf normal orientation function, $g_{\text{L}}(\theta)$ (average over all grid data). Panel (d) shows the mean projection of leaf normals to direction θ, $G(\theta)$ (average over all grid data).

(Fig. 6b). The retrieved leaf normal distribution, $g_L(\theta_L)$ has minimal variability through all grid site cell locations (Fig. 6c); and has low sensitivity to input parameters to Fredholm method. The mean projection of leaf normals exhibits the same property (Fig. 6d) and is approximately equal to 0.5 for the whole range of polar angles θ, which in classical theory corresponds to a spherical leaf normal distribution. However, according to standard RT theory $g_L(\theta_L)=1$ in for spherical leaf normal distribution, which conflict with our retrievals; consequently, we cannot call the observed leaf normal distribution spherical.

5. Variation of FPAR with SZA in heterogeneous vegetation canopies

Most models of primary productivity run on a monthly time step to simulate seasonal patterns in net plant carbon fixation, biomass, nutrient allocation and litterfall (Melillo et al., 1993; Patron et al., 1993; Prince, 1991). In recent decades, satellite data were extensively used to obtain global estimates of variables descriptive of terrestrial primary productivity. The normalized difference vegetation index (NDVI) from the advanced very high-resolution radiometer (AVHRR) has been used to estimate net primary production (NPP) and seasonal exchanges of CO_2 between the atmosphere and the terrestrial biosphere (Fung, Tucker, & Prentice, 1987; Heinmann & Keeling, 1989; Tucker, Fung, Keeling, & Gammon, 1986). Many of the fundamental questions about the global carbon cycle (its spatial variation, trends, quantification of sources and sinks) can be addressed using simulations models that operate on a scale that links remote sensing, spatial data bases of climate and soils and mechanistic understanding of atmosphere–plant–soil biogeochemistry. For instance, the Carnegie–Ames–Stanford approach (CASA), estimates spatially (1°) and temporally (monthly) averaged net ecosystem productivity on the basis of FPAR retrieved from the AVHRR NDVI data, climatological data sets (temperature and precipitation) (Potter et al., 1993). However, it is well known that FPAR changes with solar zenith angle (SZA), but most algorithms (such as the MODIS LAI and FPAR algorithm) retrieve instantaneous estimates of FPAR. A question arises as to how the remote sensing FPAR compares with FPAR estimate required by these models? Also, how do uncertainties associated with diurnal variation in FPAR compare to uncertainties from spatial variations in FPAR within coarse resolution pixels?

We address these questions by starting with the definition of FPAR (Knyazikhin, Martonchik, Myneni, et al., 1998)

$$\mathrm{FPAR}=\frac{\int_{400\ \mathrm{nm}}^{700\ \mathrm{nm}} a(\lambda)\cdot E_0(\lambda)\mathrm{d}\lambda}{\int_{400\ \mathrm{nm}}^{700\ \mathrm{nm}} E_0(\lambda)\mathrm{d}\lambda},$$

where $E_0(\lambda)$ is the solar irradiance spectrum, $a(\lambda)$ is canopy absorptance. Taking into account the law of energy conservation, absorptance can be calculated from measurements of top of canopy reflectance $r(\lambda)$ and bottom of canopy transmittance $t(\lambda)$ as $a(\lambda)=1-t(\lambda)-r(\lambda)$. Thus, it is convenient to rewrite the above as

$$\mathrm{FPAR}=1-\frac{\int_{400\ \mathrm{nm}}^{700\ \mathrm{nm}} (r(\lambda)+t(\lambda))\cdot E_0(\lambda)\mathrm{d}\lambda}{\int_{400\ \mathrm{nm}}^{700\ \mathrm{nm}} E_0(\lambda)\mathrm{d}\lambda}. \quad (24)$$

Note that the absorptance, reflectance and transmittance, and consequently FPAR, depend on LAI and the solar zenith angle, SZA. The latter introduces diurnal variations in FPAR. This dependence complicates estimation of FPAR and its validation with field data. According to our measurements at the Harvard Forest, the dependence of FPAR on solar angle was dominated by variations in FPAR due to spatial heterogeneity in the forest (dependence on LAI). Canopy FPAR was approximated from

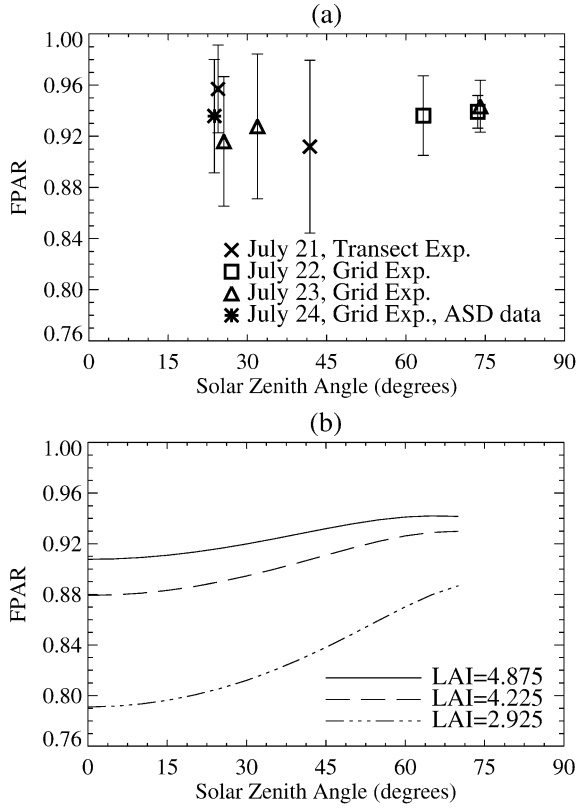

Fig. 7. Panel (a) shows FPAR estimated at different solar zenith angles (SZA) and spatial locations (grid site and transect data). Panel (b) shows the modeled dependence of FPAR on SZA for different values of LAI. FPAR variations due to LAI changes are comparable to variations due to SZA for grid site.

measured above understory canopy transmittance (Fig. 2b) and top of canopy reflectance (Fig. 2c) according to Eq. (24). We are neglecting here small contribution to FPAR from reflected by understory PAR (Goward & Huemmrich, 1992). The transmittances were not simultaneously measured at all the grid cells but at substantially different times, that is, under varying SZA. The FPAR for different sampling locations is shown in Fig. 7a as a function of SZA. For instance, one set of grid measurements were taken when SZA was 32° (cells A1–G6) and others when SZA was 65° (cells G7–I9). We see that the mean FPAR differs very little between these two measurements.

The relative influence of LAI and SZA on FPAR can be demonstrated with the help of a radiation model. FPAR was calculated with a stochastic model (Shabanov et al., 2000) for SZA varying from 0° to 70°, and a set of LAI values, 2.9, 4.2, 4.9 (at the grid site, the LAI varied from 3 to 6 and SZA varied from 25° to 72°). The optical properties of leaves used in the model correspond to that of the dominant species, sugar maple (Fig. 2a); the soil reflectance corresponds to averaged values, observed at the grid site for the corresponding values of LAI (Fig. 2d). The ratio of direct to total incident radiation was 0.5. Function G was set to 0.5, based on analysis presented previously (Fig. 6d). The results, shown in Fig. 7b, support the hypothesis that variations in FPAR due to spatial heterogeneity, that is due to variations in LAI, are larger or comparable to SZA-related variations. The SZA effect is considerably weaker in dense heterogeneous canopies. If this is a generally valid result, the use of remote sensing estimates of FPAR in ecosystem models, which typically have long time steps (weeks and months), is justified. However, these models need to address the issue of sub-pixel FPAR heterogeneity.

6. Conclusions

The research described in this paper is aimed at investigating the validity of the radiative transfer assumptions underlying of the MODIS LAI and FPAR algorithm for the case of broadleaf forests. Data collected at the EOS core validation site, Harvard Forest were used for this purpose. The parameterization of the algorithm is grounded on the concept of spectral invariants of transport equation (p_t and q_t parameters). These parameters can be evaluated from field measurements of vegetation canopy transmittances and leaf optical properties. The physical interpretation of these parameters was established. The p_t parameter is the portion of uncollided radiation in total transmitted radiation, normalized by leaf albedo. An approach to minimize the uncertainties due to spatial heterogeneity of natural vegetation in the retrievals of spectral invariants was detailed. Next, the theoretical basis of the algorithm was refined by applying stochastic concepts to radiative transfer to describe the q_t parameter. This approach accounts for the effect of foliage clumping and discontinuities, which has significant impact on LAI retrievals. The clumping coefficient was found to be inversely proportional to the probability of finding foliage elements. Finally, the effect of spatial heterogeneity was further analyzed in application to FPAR. Numerical simulations and analysis of the field data indicate that variations in FPAR due to dependency on solar zenith angle are comparable to the uncertainties in field measurements of FPAR due to spatial heterogeneity. This result supports a static representation of FPAR over broadleaf forests in large-scale ecosystem modeling.

Acknowledgements

The authors thank L. Zhou and Y. Zhang for their help with collecting field data. Financial support for this research was provided by NASA through MODIS contract NAS5-96061; we gratefully acknowledge this support.

Appendix A. Nomenclature

H	total height of canopy (m)
$\mu(\theta)$	absolute value of the cosine of direct solar radiation
L	Leaf area index
d_L	one-sided leaf area per unit volume (m^2/m^3)
FPAR	fraction of photosynthetically active radiation absorbed by the vegetation
$E_0(\lambda)$	solar irradiance spectrum ($W \cdot m^{-2} \cdot \mu m^{-1}$)
$t(\lambda)$	spectral canopy transmittance
$r(\lambda)$	spectral canopy reflectance
$\omega(\lambda)$	spectral leaf albedo
$P(\theta)$	gap fraction observed along the direction θ
$g_L(\theta_L)$	probability density of leaf normal orientation (sr^{-1})
$G(\theta)$	mean projection of leaf normals to direction θ
$Q(L, \theta)$	uncollided radiation (radiance, normalized by incoming flux; sr^{-1})
$Q^U(L, \theta)$	uncollided radiation, averaged over the vegetated portion of a horizontal plane L (radiance, normalized by incoming flux; sr^{-1})
$p(\xi)$	probability of finding foliage elements on a horizontal plane ξ
$K(L, \xi, \theta)$	correlation between foliage elements located at L and ξ along the direction θ
q_t	spectral invariant, hemispherically integrated $Q(L, \theta)$ or $Q^U(L, \theta)$
p_t	spectral invariant, eigenvalue derived in transport theory

Appendix B. Derivation of the q_t parameter

In the derivations below, we follow Zhang, Shabanov, Knyazikhin, and Myneni (2001). Consider the 1-D radiative

transfer equation for light propagation in a vegetation canopy

$$\mu(\vec{\Omega})\cdot\frac{\partial I(\lambda,L,\vec{\Omega})}{\partial L}+G(L,\vec{\Omega})\cdot I(\lambda,L,\vec{\Omega}) = \omega(\lambda)\cdot\int_{4\pi}\frac{\Gamma(L,\vec{\Omega}'\rightarrow\vec{\Omega})}{\pi\cdot\omega(\lambda)}\cdot I(\lambda,L,\vec{\Omega}')\mathrm{d}\vec{\Omega}', \quad \text{(B.1A)}$$

with boundary conditions

$$\begin{cases} I(\lambda,L_{\text{top}}=0,\vec{\Omega})=d(\vec{\Omega}), \ \ \mu(\vec{\Omega})<0, \\ I(\lambda,L_{\text{bottom}},\vec{\Omega})=0, \ \ \mu(\vec{\Omega})>0. \end{cases} \quad \text{(B.2)}$$

Here $I(\lambda,L,\vec{\Omega})$ is the radiance, L is LAI, L_{top} and L_{bottom} are LAI at the upper and lower boundary of the vegetation, respectively, λ is wavelength, $\vec{\Omega}$ is direction, $\mu(\vec{\Omega})$ is the cosine of solar zenith angle (not absolute value as in the main text), $G(\vec{\Omega})$ is the mean projection of leaf normals to the direction $\vec{\Omega}$, and $\omega(\lambda)$ is leaf albedo. It will be convenient to introduce the following operator notation with the differential $\hat{D}$ and integral $\hat{S}$ operators defined as

$$\hat{D}I(\lambda,L,\vec{\Omega})=\mu(\vec{\Omega})\cdot\frac{\partial I(\lambda,L,\vec{\Omega})}{\partial L}+G(L,\vec{\Omega})\cdot I(\lambda,L,\vec{\Omega}), \quad \text{(B.3A)}$$

$$\hat{S}I(\lambda,L,\vec{\Omega})=\int_{4\pi}\frac{\Gamma(\vec{r},\vec{\Omega}'\rightarrow\vec{\Omega})}{\pi\cdot\omega(\lambda)}\cdot I(\lambda,L,\vec{\Omega}')\mathrm{d}\vec{\Omega}'. \quad \text{(B.3B)}$$

Eq. (B.1A) can thus be rewritten as

$$\hat{D}I(\lambda,L,\vec{\Omega})=\omega(\lambda)\cdot\hat{S}I(\lambda,L,\vec{\Omega}). \quad \text{(B.1B)}$$

In the following derivations, we assume that the ratio of leaf transmittance to leaf albedo, ζ, to be independent of wavelength. Spectral variation of operator $\hat{S}$ is expressed through ζ; consequently, the operator is also wavelength independent. Note that the operators do not depend on leaf albedo. The solution $I(\lambda,L,\vec{\Omega})$ of Eqs. (B.1A,B) and (B.2) can be represented as the sum of two components, $I(\lambda,L,\vec{\Omega})=Q(L,\vec{\Omega})+\varphi(\lambda,L,\vec{\Omega})$. The first term multiplied by $|\mu(\vec{\Omega})|$, the wavelength independent function $|\mu(\vec{\Omega})|\cdot Q(L,\vec{\Omega})$, is the probability density that a photon in the incoming beam will arrive at the lower boundary of vegetation along the direction $\vec{\Omega}$ without suffering any collisions. It satisfies the equation

$$\hat{D}Q(L,\vec{\Omega})=0, \quad \text{(B.4)}$$

and boundary conditions specified by Eq. (B.2). The second term describes photons scattered one or more times in the canopy. It satisfies $\hat{D}\varphi(\lambda,L,\vec{\Omega})=\omega(\lambda)\cdot\hat{S}\varphi(\lambda,L,\vec{\Omega})+\omega(\lambda)\cdot\hat{S}Q(L,\vec{\Omega})$ and zero boundary conditions. By letting $\hat{\mathrm{T}}=\hat{\mathrm{D}}^{-1}\hat{\mathrm{S}}$, the latter can be transformed to

$$\varphi(\lambda,L,\vec{\Omega})=\omega(\lambda)\cdot\hat{T}\varphi(\lambda,L,\vec{\Omega})+\omega(\lambda)\cdot\hat{T}Q(L,\vec{\Omega}). \quad \text{(B.5)}$$

Substituting $\varphi(\lambda,L,\vec{\Omega})=I(\lambda,L,\vec{\Omega})-Q(L,\vec{\Omega})$ into this equation results in an integral equation for $I(\lambda,L,\vec{\Omega})$,

$$I(\lambda,L,\vec{\Omega})-\omega(\lambda)\cdot\hat{T}I(\lambda,L,\vec{\Omega})=Q(L,\vec{\Omega}). \quad \text{(B.6)}$$

Because $Q(L,\vec{\Omega}_0)$ does not depend on the leaf albedo, the left-hand side of Eq. (B.6) is independent of the leaf albedo, i.e.,

$$I(\lambda_1,L,\vec{\Omega})-\omega(\lambda_1)\cdot\hat{T}I(\lambda_1,L,\vec{\Omega}) = I(\lambda_2,L,\vec{\Omega})-\omega(\lambda_2)\cdot\hat{T}I(\lambda_2,L,\vec{\Omega})\equiv Q(L,\vec{\Omega}). \quad \text{(B.7)}$$

Multiplying Eq. (B.7) by $|\mu(\vec{\Omega})|$, integrating over all downward directions and considering the solution at the lower boundary of vegetation, we obtain a spectral invariant which involve transmittances $t(\lambda)$,

$$t(\lambda_1)-\omega(\lambda_1)\cdot p_{\text{t}}\cdot t(\lambda_1)=t(\lambda_2)-\omega(\lambda_2)\cdot p_{\text{t}}\cdot t(\lambda_2)\equiv q_{\text{t}}, \quad \text{(B.8)}$$

where p_{t} is a constant and

$$q_{\text{t}}\equiv\int_{2\pi^-}|\mu(\vec{\Omega})|\cdot Q(L,\vec{\Omega})\mathrm{d}\vec{\Omega} \quad \text{(B.9)}$$

is the wavelength independent parameter of interest. The physical meaning q_{t} is as follows: it denotes the probability density that a photon incident on the upper boundary of the vegetation will arrive at the lower boundary without suffering any collisions at all. Note, Q is defined for the so-called black soil problem, i.e., perfectly absorbing background.

Appendix C. WWW sites

WWW 1: EOS science plan, http://eospso.gsfc.nasa.gov/science_plan/index.php.

WWW 2: EOS core validation sites, http://modarch.gsfc.nasa.gov/MODIS/LAND/VAL.

WWW 3: Harvard Forest site, http://lternet.edu/hfr/.

References

Bonan, G. B. (1998). The Land Surface Climatology of the NCAR Land Surface Model coupled the NCAR Community Climate Model. *Journal of Climate*, *11*, 1307–1327.

Chen, J. M. (1996). Optically based methods for measuring seasonal variations in leaf area index in boreal conifer stands. *Agricultural and Forest Meteorology*, *80*, 135–163.

Chen, J. M., Rich, P. M., Gower, S. T., Norman, J. M., & Plummer, S. (1997). Leaf area index of broadleaf forests: theory, techniques, and measurements. *Journal of Geophysical Research*, *101*(D24), 29429–29443.

Dickinson, R. E., Henderson-Sellers, A., Kennedy, P. J., & Wilson, M. F. (1986). Biosphere–Atmosphere Transfer Scheme (BATS) for the NCAR CCM, NCAR/TN-275-STR. Boulder, CO: NCAR Research.

Fung, I. Y., Tucker, C. J., & Prentice, K. C. (1987). Application of advanced very high resolution radiometer vegetation index to study of atmosphere–biosphere exchanges of CO_2. *Journal of Geophysical Research*, *92*, 2999–3015.

Goward, S. N., & Huemmrich, K. F. (1992). Vegetation canopy par absorptance and the normalized difference vegetation index—an assessment using the sail model. *Remote Sensing of Environment*, *39*(2), 119–140.

Heinmann, M., & Keeling, C. D. (1989). A three dimensional model of atmospheric CO_2 transport based on observed winds: II. Model description. In D. H. Peterson (Ed.), *Aspects of climate variability in the Pacific and Western AmericaGeophysical Monograph Series vol. 55* (pp. 240–260).

Justice, C., Belward, A., Morisette, J., Lewis, P., Privette, J., & Baret, F. (2000). Developments in the 'validation' of the satellite sensor products for the study of the land surface. *International Journal of Remote Sensing*, *21*(17), 3383–3390.

Knyazikhin, Y., & Marshak, A. (1991). In R. B. Myneni, & J. Ross (Eds.), *Photon–vegetation interactions. Applications in optical remote sensing and plant ecology.* Berlin-Heidelberg: Springer-Verlag (Chapter 1).

Knyazikhin, Y., Martonchik, J. V., Diner, D. J., Myneni, R. B., Verstraete, M., Pinty, B., & Gobron, N. (1998). Estimation of vegetation canopy leaf area index and fraction of absorbed photosynthetically active radiation from atmosphere-corrected MISR data. (EOS-AM1 Special Issue of) *Journal of Geophysical Research*, *103*(D24), 32239–32257.

Knyazikhin, Y., Martonchik, J. V., Myneni, R. B., Diner, D. J., & Running, S. W. (1998). Synergistic algorithm for estimating vegetation canopy leaf area index and fraction of absorbed photosynthetically active radiation from MODIS and MISR data. *Journal of Geophysical Research*, *103*(D24), 32257–32277.

Melillo, J. M., McGuire, A. D., Kicklighter, D. W., Moore, B., Vorosmatry, C. J., & Schloss, A. L. (1993). Global climate change and terrestrial net primary productivity. *Nature*, *363*, 234–240.

Miller, J. B. (1964). An integral equation for phytology. *Journal of the Australian Mathematical Society*, *4*, 397–402.

Miller, J. B. (1967). A formula for average foliage density. *Australian Journal of Botany*, *15*, 141–144.

Myneni, R. B., Hoffman, S., Knyazikhin, Y., Privette, J. L., Glassy, J., Tian, Y., Wang, Y., Song, X., Zhang, Y., Smith, G. R., Lotsch, A., Friedl, M., Morisette, J. T., Votava, P., Nemani, R. R., & Running, S. W. (2002). Global products of vegetation leaf area and fraction absorbed PAR from year one of MODIS data. *Remote Sensing of Environment*, *83*, 214–231.

Nilson, T. (1971). A theoretical analysis of the frequency of gaps in plant stands. *Agricultural Meteorology*, *8*, 25–38.

Norman, J. M., & Campbell, G. S. (1989). W. Pearcy, et al. (Ed.), *Plant physiological ecology* (pp. 301–325). Chapman & Hall.

Panferov, O., Knyazikhin, Y., Myneni, R. B., Szarzynski, J., Engwald, S., Schnitzler, K. G., & Gravenhorst, G. (2001). The role of canopy structure in the spectral variation of transmission and absorption of solar radiation in vegetation canopies. *IEEE Transactions on Geoscience and Remote Sensing*, *39*(2), 241–253.

Patron, W. J., Scurlock, J. M. O., Ojima, D. S., Gilmanov, T. G., Scholes, R. J., Schimel, D. S., Kirchner, T., Menaut, J.-C., Seastedt, T., Moya, E. G., Kamnalrut, A., & Kinyamario, J. I. (1993). Observations and modeling of biomass and soil organic matter dynamics for the grassland biome worldwide. *Global Biogeochemical Cycles*, *7*(4), 785–809.

Phillips, D. L. (1962). A technique for numerical solution of certain integral equations of the first kind. *Journal of the Association for Computing Machinery*, *9*, 84–97.

Potter, C. S., Randerson, J. T., Field, C. B., Matson, P. A., Vitousek, P. M., Mooney, H. A., & Klooster, S. A. (1993). Terrestrial ecosystem production: a process model based on global satellite and surface data. *Global Biogeochemical Cycles*, *7*(4), 811–841.

Prince, S. D. (1991). A model of regional primary production for use with coarse-resolution satellite data. *International Journal of Remote Sensing*, *12*, 1313–1330.

Privette, J. L., Myneni, R. B., Knyazikhin, Y., Mukelabai, M., Roberts, G., Tian, Y., Wang, Y., & Leblanc, S. G. (2002). Early spatial and temporal validation of MODIS LAI product in the Southern Africa Kalahari. *Remote Sensing of Environment*, *83*, 232–243.

Ross, J. (1981). The radiation regime and architecture of plant stands. . Hague: Dr. W. Junk Publishers.

Running, S. W., & Coughlan, J. C. (1988). A general model of forest ecosystem processes for regional applications. *Ecological Modelling*, *42*, 124–154.

Sellers, P. J., Randall, D. A., Collatz, G. J., Berry, J. A., Field, C. B., Dazlich, D. A., Zhang, C., Collelo, G. D., & Bounoua, L. (1996). A revised land surface parameterization (SIB2) for Atmospheric GCMs: Part I. Model formulation. *Journal of Climate*, *9*, 676–705.

Shabanov, N., Knyazikhin, Y., Baret, F., & Myneni, R. B. (2000). Stochastic modeling of radiation regime in discontinuous vegetation canopies. *Remote Sensing of Environment*, *74*, 125–144.

Thomlinson, J. R., Bolstad, P., & Cohen, W. (1999). Coordinating methodologies for scaling land cover classification from site specific to global; steps towards validating globally based map products. *Remote Sensing of Environment*, *70*, 16–28.

Tian, Y., Woodcock, C. E., Wang, Y., Privette, J., Shabanov, N. V., Zhou, L., Zhang, Y., Buuermann, W., Dong, J., Veikkanen, B., Hame, T., Anderson, K., Ozdogan, M., Knyazikhin, Y., & Myneni, R. B. (2002a). Multiscale analysis and validation of the MODIS LAI product I. Uncertainty assessment. *Remote Sensing of Environment*, *83*, 414–430.

Tian, Y., Woodcock, C. E., Wang, Y., Privette, J., Shabanov, N. V., Zhou, L., Zhang, Y., Buuermann, W., Dong, J., Veikkanen, B., Hame, T., Anderson, K., Ozdogan, M., Knyazikhin, Y., & Myneni, R. B. (2002b). Multiscale analysis and validation of the MODIS LAI product II. Sampling strategy. *Remote Sensing of Environment*, *83*, 431–441.

Tian, Y., Zhang, Y., Knyazikhin, Y., Myneni, R., Glassy, J., Dedieu, G., & Running, S. (2000). Prototyping of MODIS LAI and FPAR algorithm with LASUR and LANDSAT data. *IEEE Transactions on Geoscience and Remote Sensing*, *38*(5), 2387–2401.

Tikhonov, A., & Arsenin, V. (1977). Solutions of ill-posed problems. Washington, DC: V.H. Winston and Sons.

Tucker, C. J., Fung, I. Y., Keeling, C. D., & Gammon, R. H. (1986). Relationship between atmospheric CO_2 variations and satellite-derived vegetation index. *Nature*, *319*, 195–199.

Vainikko, G. M. (1973). Transfer approach to the mean intensity of radiation in noncontinuous clouds. *Trudy MGK SSSR, Meteorological Investigations*, *21*, 38–57 (in Russian).

Wang, Y., Tian, Y., Zhang, Y., El-Saaleous, N., Knyazikhin, Y., Vermote, R., & Myneni, R. (2001). Investigation of product accuracy as a function of input and model uncertainties: case study with SeaWiFS and MODIS LAI/FPAR algorithm. *Remote Sensing of Environment*, *78*, 296–311.

Wang, Y., Woodcock, C. E., Buermann, W., Stenberg, P., Voipio, P., Smolander, H., Hame, T., Tian, Y., Hu, J., Knyazikhin, Y., & Myneni, R. B. (2002). Validation of the MODIS LAI product in coniferous forests of Ruokolahti, Finland. *Remote Sensing of Environment*, (in preparation).

Wilson, W. (1960). Inclined point quadrats. *The New Phytologist*, *59*, 1–5.

Zhang, Y., Shabanov, N. V., Knyazikhin, Y., & Myneni, R. B. (2001). Assessing information content of multiangle satellite data for mapping biomes: II. Theory. *Remote Sensing of Environment*, *80*, 1–12.

Zhang, Y., Tian, Y., Knyazikhin, Y., Martonchik, J. V., Diner, D. J., Leroy, R., & Myneni, R. (2000). Prototyping of MISR LAI and FPAR algorithm with POLDER data over Africa. *IEEE Transactions on Geoscience and Remote Sensing*, *38*(5), 2402–2418.